Reliable Lifting Surface Solutions for Unsteady Flow

Peter F. Jordan*
Martin Marietta Laboratories, Baltimore, Md.

Numerical experimentation has shown that accurate solutions, obtained for suitable sets of numbers N^2 of finite elements, can readily be extrapolated to the limit $N=\infty$ and thus to the correct solution for the given wing. A method for calculating the required accurate solutions, even in the case of unsteady flow, has been developed. As a sample application, the gust load admittance function is calculated for a set of rectangular wings and, by means of further extrapolation, presented for all reduced frequencies k and for all aspect ratios in the range $A=1$ to $A=\infty$. Additional sample results presented are flutter coefficients and an admittance value for a chessboard-type gust field.

Introduction

IN general, numerical solutions to lifting surface problems tend to be of uncertain accuracy. For steady flow, however, the following approach has been successful: represent the given wing by a number N^2 of finite elements. This "model problem" can be solved to arbitrary accuracy; its solution is not an accurate solution of the given wing problem, but the inaccuracy is due to the difference between wing and model. Hence, select a suitable set of numbers N, calculate the accurate solution for each, and extrapolate over $(1/N)$ to the limit $(1/N)=0$. In our experience, this extrapolative procedure is quite successful; extrapolation is smooth, almost linear, and the limit result can be considered as the sought-for reliable solution of the original wing problem. This is described in more detail in the first part of the next section.

In the general case of unsteady (harmonic) flow, the same extrapolative procedure did not seem possible, because here accurate solutions of such model problems were not readily available. For example, it is shown in Ref. 1 that in the widely used doublet-lattice method the "corner error" tends to grow as N is increased; therefore, extrapolation becomes a doubtful proposition. However, we have developed a new method, outlined in Ref. 1, which allows one to accurately solve unsteady flow model problems. This new method is described in the Appendix of this paper.

After computerizing our new method, we explored to see if extrapolation behaves as smoothly and reliably in unsteady flow problems as it did in steady flow analyses. In our experience so far (with relatively simple problems), this has always been the case. The main problem with which we have dealt is a basic problem of long standing and of considerable practical interest, namely, the generalization of the classical gust load problem (the problem for which the Sears function $\phi(k)$ is the solution) to rectangular wings of finite aspect ratios A, down to $A=1$. Simultaneously, we obtained the results for the companion problem—the wing exposed to a uniform oscillating downwash. The latter results are essentially flutter coefficients; the extrapolative procedure performed entirely satisfactorily both with these and with the gust load results.

For standard gust response calculations, one requires the gust loads in the form of an admittance function; we present our results in this form also. In both of its parameters, reduced frequency k and aspect ratio A, this function behaves so regularly that, by means of further extrapolations, we have been able to cover the full parameter range, up to $k=\infty$ and between $A=1$ and $A=\infty$. This is satisfying because so far only scanty information has been available about the aspect ratio effect on gust loading, justifying our endeavor to obtain primary results of rather higher accuracy than required in routine gust response calculations.

Our investigation (as far as reported here) deals with rectangular finite elements, with planar wings, and with incompressible flow. The description of the analysis in the Appendix is confined to this range of applications.

Presented as Paper 78-228 at the AIAA 16th Aerospace Sciences Meeting, Huntsville, Ala., Jan. 16-18, 1978; submitted Feb. 2, 1978; revision received May 3, 1978.

Index categories: Nonsteady Aerodynamics; Computational Methods.

*Consultant. Associate Fellow AIAA.

Technical Discussion

Steady Flow Results

Steady flow lift coefficients C_L for unit incidence ($\alpha=1$) are plotted in Fig. 1 over the reciprocal aspect ratio $(1/A)$, both for elliptic and rectangular wings. (C_L/π rather than C_L itself is plotted for convenience.) For elliptic wings, the Helmbold curve is plotted, simply to illustrate the interesting fact that the C_L curves for elliptic and rectangular wings differ rather little (as one might already suspect from comparing Figs. VIII.26 and 28 in Ref. 2).

For rectangular wings, results of finite element analyses are plotted for $A=1$, 2, 3, and 6. For these analyses, each wing was subdivided into $N\times N$ equal rectangular elements. Results obtained, using the Falkner horseshoe vortex as the finite element (see, e.g., Ref. 3), are shown for $N=2$, 4, 6, and 12.

Results for $N=\infty$ (i.e., results that are supposed to be the correct results for the given wings rather than for their models) are also shown in Fig. 1; these were obtained by parabolic extrapolation in the coordinate $(1/N)$ of the results for $N=4$, 6, and 12. Thus, the extrapolation takes the form

$$R_\infty = R_4 - 3R_6 + 3R_{12} \tag{1}$$

Note that the numbers 4, 6, 12, and ∞ form an equidistant sequence in $(1/N)$. The fact that the respective results plot as almost equidistant points in all four sets in Fig. 1 indicates that the extrapolating parabolas were almost straight lines.

According to Fig. 1, the results for $N=12$ (obtained with 144 finite elements) are still noticeably different from the results for $N=0$; the error is 7.5% for $A=1$, decreasing to 4.9% for $A=6$ (and, of course, to zero when $(1/A)\to 0$). The magnitude of the errors when A is finite may be somewhat surprising; however, the near-linearity of the interpolative curves (which was well confirmed by controls obtained with additional values N) supports the validity of the procedure. In order to obtain an independent confirmation, we repeated the analysis for $A=1$ with a markedly different finite element—the Woodward[4] element (modified by shifting its collocation point forward to the 85% chord position). For finite N, the two sets of results were different, but the two end results

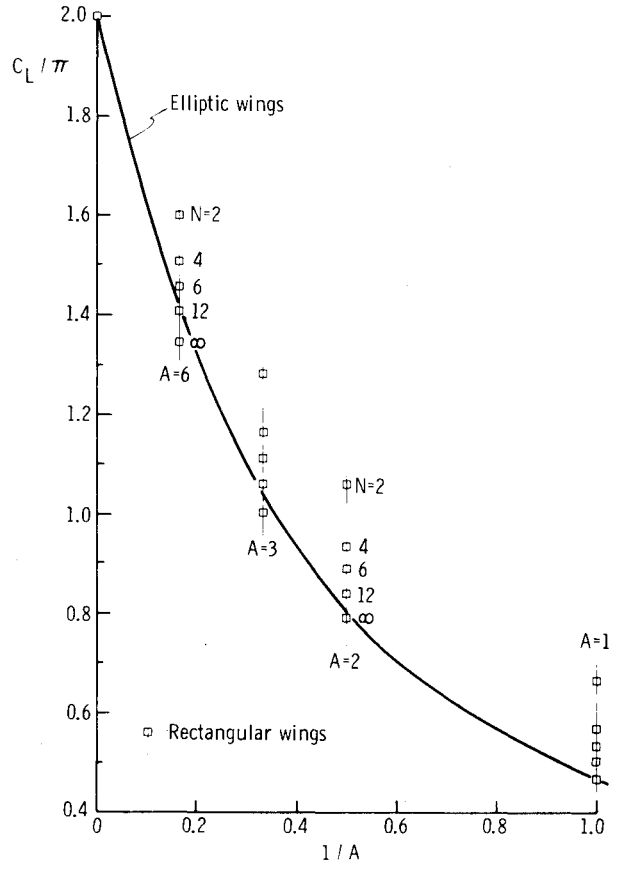

Fig. 1 Steady flow results.

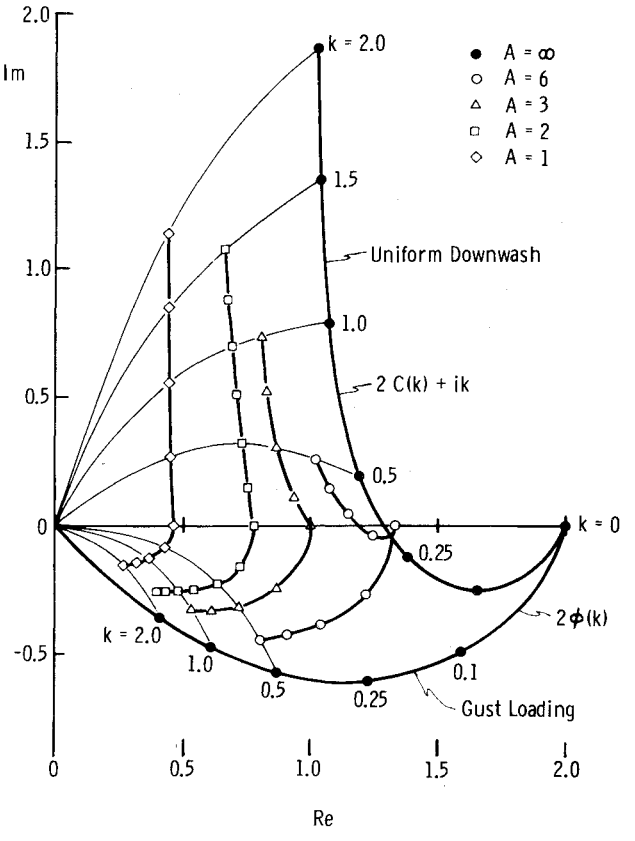

Fig. 2 Lift coefficients C_L/π in unsteady flow.

agreed to within the estimated accuracy of the numerical work†:

$$C_{L(N=\infty)} = \left\{\begin{matrix} 1.46000 \text{ (Falkner element)} \\ 1.46008 \text{ (Woodward element)} \end{matrix}\right\} \text{(square wing)} \quad (2)$$

Additional confirmation of the validity of our extrapolative results is contained in Table 1 of a recent paper by Graham,[5] which lists steady flow results for rectangular wings obtained by several authors using different methods. Comparing the supposedly most accurate of these results with ours, we have Table 1. The difference of 0.5% for $A=6$ is readily explained: The value 4.199 is Graham's "first approximation" and is not expected to be very accurate.

Unsteady Flow Results

The complex-valued lift coefficients for finite aspect ratios A which are plotted in Fig. 2 are final values, corresponding to $N=\infty$ in Fig. 1. They refer to the same set of rectangular wings for which the $k=0$ results are shown in Fig. 1, and are simply extensions of these results into two types of unsteady flow: 1) the sinusoidal gust, stationary in space, infinitely extended and aligned with the wing span, and 2) the wing exposed to an oscillatory downwash that is uniformly distributed over the wing. Unit downwash amplitude, corresponding to $\alpha=1$ in steady flow, is assumed; reference line for the gust phase is the leading edge. The reduced frequency k is referred to the wing half-chord; i.e., $k \equiv k_{c/2}$.

Plotted for comparison are the corresponding classical results for $A=\infty$; that is, the curves of the functions

$$C_L/\pi = \left\{\begin{matrix} 2\phi(k) & \text{(gust loading)} \\ 2C(k)+ik & \text{(uniform downwash)} \end{matrix}\right\} (A=\infty) \quad (3)$$

where $\phi(k)$ is the Sears function, referred to the leading edge, and $C(k)$ is the Theodorsen function.

The curves for different A-values are identified by different symbols. All curves start from the positive real (Re) axis where $k=0$. All gust load curves dip downward into the range of negative imaginary (Im) values. Extended farther, these curves would turn upward and would reach the point of origin (where $k=\infty$), presumably within the angle between the curve $2\phi(k)$ and the Re axis. Of the curves for uniform downwash, those for $A=\infty$ and $A=6$ also dip downward at first but both soon reverse, crossing the Re axis and ascending with increasing steepness. The curves for smaller A ascent immediately.

The k-values are indicated along both curves for $A=\infty$. The k-values along the curves for finite A are readily inferred from the interpolative curves for constant k which are drawn between the curves $A=\infty$ and the point of origin, noting that, for each finite A, the steps Δk between consecutive points are uniform (e.g., $\Delta k=0.25$ along both curves for $A=2$).

The primary analyses, with $N=4$, 6, and 12, from which the results shown in Fig. 2 have been obtained by means of Eq. (1), are described in the Appendix. Demonstrated in Figs. 3a (gust) and 3b (uniform) is how this extrapolative procedure performed in the present two types of unsteady flow. In Fig. 3a, the extrapolative curves are almost straight lines which are

Table 1 Comparison of C_L values

Author	$A=1$	$A=2$	$A=6$
Graham	1.460 or 1.461	2.474	4.199
Jordan	1.4600 or 1.4601	2.4740	4.2206

† The agreement that is shown in Eq. (2) can also be taken as a general confirmation of the finite element method.

subdivided by the N-curves into almost equal parts. This corresponds closely to the extrapolations shown in Fig. 1. In Fig. 3b, the N-curves cross each other and, consequently, the curve for $k=1.5$ is highly curved. However, this can hardly cast doubt on the validity of the procedure, since the resultant curve, $N=\infty$, is quite smooth and almost a straight line. The performances shown in Figs. 3a and 3b are those with $A=1$; those with other aspect ratios are quite similar and are not shown.

The curves in Fig. 2 are interesting in a number of respects. Their regularity tends to encourage further inter- and extrapolations which, for the gust load case, will be demonstrated in the next section.

An interesting observation resulted from reviewing the chordwise lift distributions due to gust loadings. An intriguing property of the classical solution for $A=\infty$ is that, while the load, the downwash, does contain chordwise phase shift, the resulting lift is free of chordwise phase shift. Unexpectedly, the same seems to hold true with finite A, even down to $A=1$. It is difficult, of course, to derive an exact result of this type. With N finite, the lift distribution is not quite uniquely defined, and extrapolation to $N=\infty$ is thus not an exact procedure. Nevertheless, the larger the N, the smaller the recognizable phase shift, and attempts to extrapolate seem to indicate that no phase shift is left when $N=\infty$.

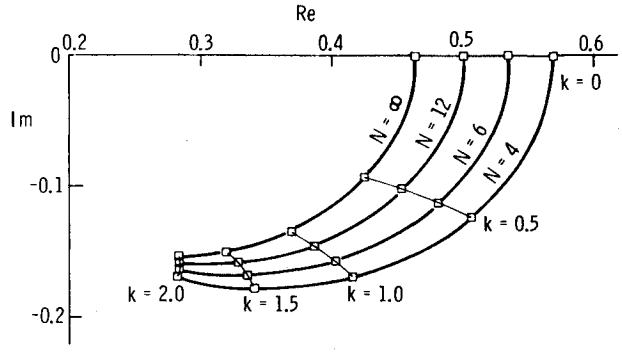

Fig. 3a Extrapolation to the $A=1$ gust curve in Fig. 2.

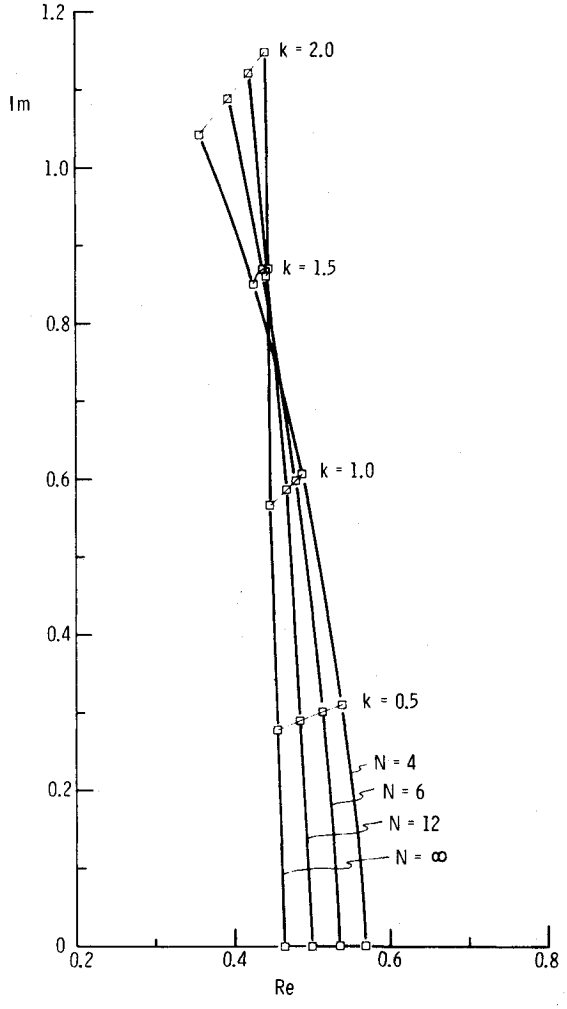

Fig. 3b Extrapolation to the $A=1$ uniform downwash curve in Fig. 2.

Gust Load Admittance Functions

The lift coefficient for $A=\infty$, $2\pi\phi(k)$, is known to go to zero when $k\to\infty$ as $k^{-1/2}$. One expects a similar singularity in the lift coefficients $C_L(k)$ for finite A. We eliminate the singularity by dividing the latter function by the former.

In a standard gust analyses, one requires only the absolute value of the complex-valued coefficient $C_L(k)$, the square of which is called the admittance function. Hence, we define the function

$$\bar{C}_L = |C_L(k)|/2\pi|\phi(k)| \tag{4}$$

the square of which, $\bar{C}_L^2$, might be called the normalized admittance function. From physical considerations, it is clear that this function must be described by a smooth curve which ascends monotonously as k increases and can, at most, reach $\bar{C}_L^2=1$ as $k\to\infty$.

For lower values of k, we calculated $\bar{C}_L$ from the $C_L(k)$ values shown in Fig. 2. Extrapolation to larger values of k was done in the coordinate $(1/k)$. Parabolic extrapolation was used:

$$\bar{C}_L = a+b/k+c/k^2 \tag{5}$$

This is demonstrated graphically for $A=1$ in Fig. 4. One sees that the parabola is almost a straight line and thus invites extrapolation up to the origin $(1/k)=0$. The end point that was reached was checked by third-order extrapolation, using the result for $(1/k)=2$ as the fourth input value. While the second-order result was $\bar{C}_L=0.6634$, the third-order result was 0.6632. The latter value is not necessarily the more accurate, but the close agreement between the two end values is comforting and may be considered as an indication that the extrapolative results should be accurate to a few units in the fourth decimal.

Table 2 lists the constants in Eq. (5) for all four aspect ratios. Note that the constant c, which measures the curvature of the parabolas, decreases quickly as A increases.

Table 2 The constants in Eq. (5)

A	a	b	c
1	0.6634	−0.1964	0.0353
2	0.8104	−0.1112	0.0121
3	0.8682	−0.0719	0.0058
6	0.9308	−0.0325	0.0018

Table 3 Normalized gust load coefficients $\bar{C}_L$

k	$A=1$	$A=2$	$A=3$	$A=6$
0	0.2324	0.3938	0.5006	0.6717
0.125				0.7777
0.25	0.3342	0.5492	0.6729	0.8299
0.375				0.8571
0.5	0.4131	0.6364	0.7474	0.8731
0.75		0.6836	0.7825	0.8907
1.0	0.5023	0.7113	0.8020	0.9001
1.5	0.5482	0.7416	0.8228	0.9099
2.0	0.5741	0.7578	0.8337	0.9150
4.0	0.6165	0.7833	0.8506	0.9228
∞	0.6634	0.8104	0.8682	0.9308

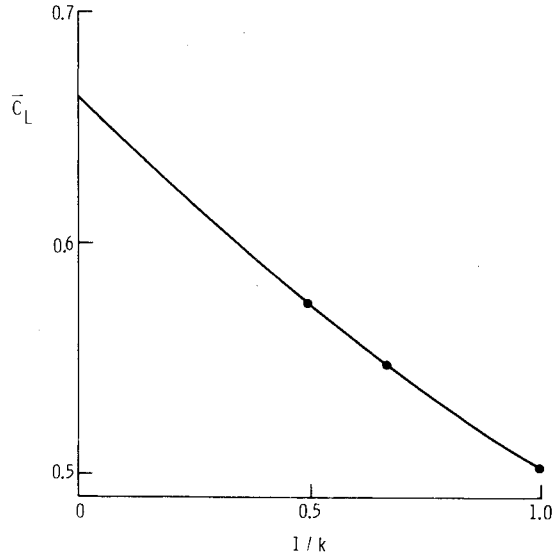

Fig. 4 Extrapolation over $(1/k)$ for $A = 1$.

Simultaneously, $|b|$ decreases. This is as it should be, since for $A \to \infty$ we must have $\bar{C}_L \equiv 1$.

Table 3 lists numerical values for $\bar{C}_L$. In each of the four sets, the values for the lower k, including the triplets of values that are indicated by brackets, are those calculated from the original $N = \infty$ results. The triplets are the bases for the extrapolations, Eq. (5), and the values for higher k are extrapolated values.[‡]

So far, we have covered the complete k range with four aspect ratios A. Interpolation with respect to A is done graphically, over the coordinate $(1/A)$, in Fig. 5. The curve for $k=0$ corresponds to the curve that might be drawn through the points for $N=\infty$ in Fig. 1. The curve for $k=\infty$ connects the results of four independent extrapolations, Eq. (5), with the theoretical value at the origin, $\bar{C}_L = 1$ when $(1/A) = 0$. The smoothness of this curve is a rather convincing confirmation of the validity of the procedure by which it was derived. The difference between this curve and the horizontal $\bar{C}_L = 1$, its theoretical maximum, is indicative of a wing tip effect which is seen to persist even as $k \to \infty$ (i.e., as the wavelength of the gusts goes to zero). However, this is not a difference in lift coefficients; rather, as $k \to \infty$, both lift coefficients in Eq. (4) (the numerator and the denominator) go to zero.

That the curve for $k = \infty$ has little curvature indicates that here the two tip effects are concentrated essentially at the tips, with little overlap between them even when $A = 1$. This agrees with what one would expect from physical considerations.

Some prior results are shown in Fig. 6. The results for elliptic wings have been derived, by means of a Fourier transformation, from the remarkable, very early results of R.T. Jones[6] for the sharp-edged gust (Eq. (45) of Ref. 6). The slight irregularities which they exhibit stem from the sensitivity of the transformation and are not of concern. Of concern is the fact that both curves descend rather than ascend beyond $k=3$ (both continue to descend beyond the k range shown in Fig. 6). This descent arises from the fact that the result of the transformation does not contain the characteristic singularity of the ϕ function (see above).

The two sets of prior results for the rectangular wing, $A=6$, in Fig. 6, the recent ones, Ref. 5 (up to $k=2.5$), and the earlier

[‡]Four decimals are given in Tables 2 and 3 simply as a matter of consistency. We estimate that the $\bar{C}_L$ values in the upper part of Table 3 should be correct to one or two units in the fourth decimal, but expect lesser accuracy from the extrapolated values. Figure 5, a suitable basis for interpolating with respect to both A and k, is an ordinary graphical interpolation but is, nevertheless, more than accurate enough for routine gust analyses.

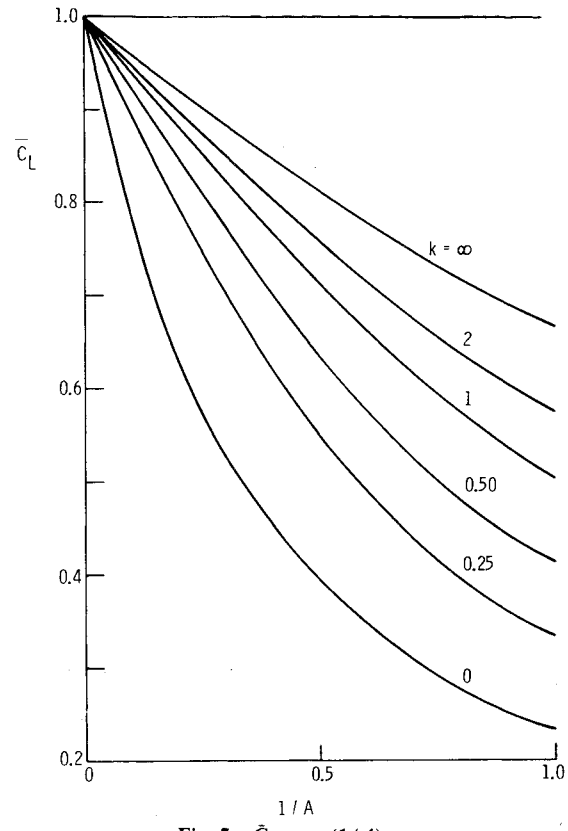

Fig. 5 $\bar{C}_L$ over $(1/A)$.

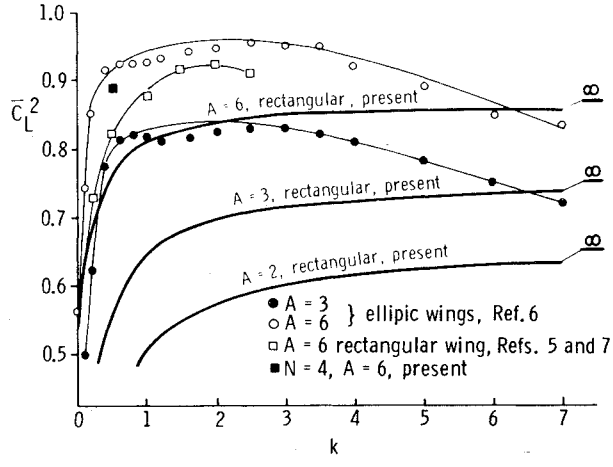

Fig. 6 Normalized gust load admittance functions.

ones, Ref. 7 (up to $k=1.0$), agree fairly well. Nevertheless, Graham,[5] who presents both sets, does not claim that they confirm each other. He does not consider the Ref. 7 results to be reliable, and his own results are again only first approximations. Their curve again exhibits a tendency to descend as k becomes large. Thus, none of these earlier results can be considered reliable.

Also shown in Fig. 6 are our present curves for rectangular wings with $A=2$, 3, and 6. A first impression is that our $\bar{C}_L^2$ values appear to be rather small, at least around $k=1$. But Fig. 6 also shows (as a solid square) our result for $N=4$ when $A=6$ and $k=0.5$. The vertical distance of this square from our $A=6$ curve demonstrates the large $\bar{C}_L^2$ range that is covered by our extrapolation to $N=\infty$. Within this distance, the result of Refs. 5 and 7 corresponds roughly to our result for $N=12$; accordingly, it is not accurate. Thus, while

Graham's first approximation is fairly accurate with steady flow (Table 1), it becomes inadequate with unsteady flow.

The two companion problems presented in Fig. 2—gust loading and uniform downwash—differ only in the downwash terms of the linear system. Thus, our experience that extrapolation to $N=\infty$ could always be performed successfully describes a property of the homogeneous part of the system; no difficulties should be encountered with different downwash terms.

While our analysis referred mainly to the classical gust load problem of one-dimensional gust fields, it is well-known that more realistic gust fields lead to greatly reduced admittances. We performed a sample analysis for a chessboard type of gust field ($A=1$, $k=2$, $N=12$). In this case, the change from a one- to a two-dimensional gust field reduced the admittance by 71%.

Conclusions

The generalization of the Sears function to rectangular wings of finite aspect ratios has been derived and is presented for the full range of gust frequencies k and for all aspect ratios down to $A=1$, the square wing. The derivation utilized extrapolation to an infinite number of finite elements. Extrapolation as such is not a new idea; however, our procedure has been based on unusually accurate primary solutions, and it fully covers a considerable range of parameters in a consistent manner. The resultant function of k and A, Fig. 5, is of remarkable regularity and gives interesting physical insight. In addition, results are presented for a flutter coefficient and a sample result for a chessboard type gust field. The flutter coefficient is given for four aspect ratios A in Fig. 2. Approximate curves for other A and for higher k values can readily be inferred.

There is an additional point of practical interest. With approximate methods, the advice is sometimes given that the aspect ratio of individual elements should not exceed $A=1$. Indeed, the error due to the "parabolic approximation" (e.g., Ref. 8) increases rapidly when the elemental A becomes larger than 1 (see, for example, Fig. 2 of Ref. 1). No corresponding error arises in our accurate method; consequently, we were able to use elements with $A=6$ without penalty. Thus, in suitable cases, our method permits a considerable reduction in the number of finite elements and thus a considerable saving of computational effort.

It remains to generalize the analysis to include compressibility, skewed elements for dealing with swept wings, etc.

Appendix: Aerodynamic Analysis

Formulation

Consider the given lifting surface to be composed of finite elements E_n. One requires the aerodynamic influence coefficients $w_{s,n}$ which measure the induced downwash, due to unit lift on any one "sending" element E_s among the E_n, on the preselected collocation points (x_n,y_n) of all E_n. In a given problem, the downwash at the (x_n,y_n) is given and the unknown lift coefficients $C_{L,s}$ of the E_s have to be determined from the requirements that, on each (x_n,y_n), the sum of all induced downwashes $w_{s,n}C_{L,s}$ must equal the given downwash. This leads to a linear system, the solution of which is the solution of the given problem.

As our model for E_s, we use the Falkner horseshoe vortex,[3] and our method may thus be called a doublet-lattice method (see, e.g., Ref. 8). However, we use a more accurate method for calculating the $w_{s,n}$. Here the presentation of this method parallels that originally given in Ref. 1 and assumes planar wings and incompressible flow. Furthermore, we assume initially that the E_n are squares of equal sizes. Generalization to rectangular elements and details of the execution are added.

As indicated in Fig. A1, the squares E_n are aligned with the undisturbed flow speed V and the coordinates x and y relate to E_s. The x axis is centered on E_s; the bound part of the horseshoe vortex spans the 1/4-chord of E_s and lies on the y axis. Both coordinates are referred to the length l which is one-half the chord length of each E_n. The collocation point on E_s is thus $(x_s,y_s)=(1,0)$ and, more generally, the x_n take only odd integer values while the y_n take only even values.

In the main part of this paper, we presented results for various wings and hence had to use a frequency parameter which referred to these wings; thus, we used $k\equiv k_{c/2}$. In this Appendix, we deal exclusively with elements E_n, and we thus need a frequency parameter k_e which refers to the E_n:

$$k_e=\omega l/V=k_{c/2}/N \tag{A1}$$

However, the distinction between the two purposes is so obvious that, in order to obtain simpler formulas, we can again drop the index, writing k for k_e. From here on, therefore, k will always mean k_e.

By unit lift (see above), we imply that the lift coefficient of E_s is

$$C_{L,s}=\exp(i\omega t) \tag{A2}$$

The influence coefficient $w_{s,n}$ measures the dimensional downwash $W_s(x_n,y_n)$ as follows:

$$\pi W_s(x_n,y_n)=Vw_{s,n}\exp(i\omega t) \tag{A3}$$

The individual coefficients $w_{s,n}$ are individual values of a continuous (in general) function $w(x,y;k)$, and it is more convenient, in our analysis, to use this functional form, given by an integral of the form

$$w(x,y;k)=-\frac{1}{4}\int_{-l}^{+l}K(x,|y-\eta|,k)\,\frac{d\eta}{(y-\eta)^2} \tag{A4}$$

All terms in Eq. (A4) are nondimensional. The kernel K is given by the integral

$$K=\int_{-x/|y-\eta|}^{\infty}\exp[-ik(x+|y-\eta|u)]\,\frac{du}{(1+u^2)^{3/2}} \tag{A4a}$$

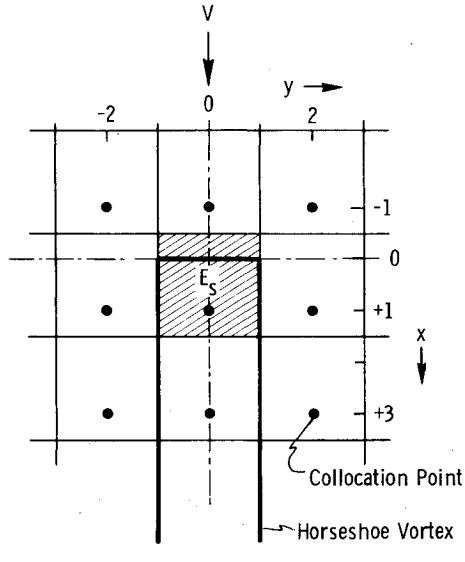

Fig. A1 Arrangement of square elements and coordinates x and y.

General

To evaluate the kernel K numerically, one has to evaluate incomplete cylinder functions. The method proposed in Appendix A of Ref. 8 is not particularly accurate. [A much more accurate (and also slightly simpler) method has been presented recently.[9]] In addition, the outer integral, Eq. (A4), is a Hadamard integral, singular to second order whenever $y=0$, and its evaluation is then particularly sensitive. Thus, there are two distinct sources of numerical error in this method of evaluation; we avoid both by choosing a different path.

We demonstrate our approach first with what is apparently the most difficult case, $y=0$, writing $w(x;k)$ for $w(x,0;k)$. Later, we show that $w(x,y;k)$ can be expressed in a simple manner by $w(x;k)$.

Equation (A4), with Eq. (A4a) inserted, presents a double integral. The essence of our approach is that we reverse the sequence of integrations. That this reversal is permitted one checks most readily in the case $k=0$. Here all integrations can be performed analytically in either sequence, and the same result is obtained either way.

Setting $y=0$, $u\eta=\zeta$, and reversing, one obtains

$$-2w(x;k)e^{ikx}=\int_{-x}^{\infty}e^{-ik\zeta}\left(\int_0^1\frac{d\eta}{(\eta^2+\zeta^2)^{3/2}}\right)d\zeta$$

$$=\int_{-x}^{\infty}\frac{e^{-ik\zeta}d\zeta}{\zeta^2(1+\zeta^2)^{1/2}}\equiv J(-x) \tag{A5}$$

The problem of determining $w(x;k)$ has been reduced to that of evaluating the integral $J(-x)$. The real and imaginary parts of this integral will be denoted as

$$J(x)=J^c(x)-iJ^s(x) \tag{A6}$$

where the suffix c indicates cos and the suffix s indicates sin in the integrand.

The integral J is not difficult to evaluate, but different methods are required in different ranges of the variable ζ. To indicate an integral that extends from $\zeta=a$ to $\zeta=b$, we write $J(a,b)$, but we usually omit the upper limit if this limit is ∞. Thus,

$$J(a)\equiv J(a,\infty)=J(a,b)+J(b) \tag{A7}$$

The singularity at $\zeta=0$ enters if x is positive but not if x is negative. To avoid confusion of signs (and a clumsy notation), we introduce p to mean $|x|$. We deal first with the case $x\leq -1$.

Case $x\leq -1$

Writing v for $k\zeta$, we have

$$J^c(p)=k^2\int_{kp}^{\infty}\frac{\cos v}{(1+(k/v)^2)^{1/2}}\frac{dv}{v^3}=\sum_{\nu=1}^{\infty}J_\nu^c(p) \tag{A8}$$

with

$$J_\nu^c(p)=(-)^{\nu-1}\overline{\nu-1}k^{2\nu}\int_{kp}^{\infty}\frac{\cos v\,dv}{v^{2\nu+1}} \tag{A8a}$$

where

$$\bar{\nu}\equiv\frac{1\cdot3\cdot5\cdots(2\nu-1)}{2\cdot4\cdot6\cdots(2\nu)};\quad(\bar{0}=1) \tag{A8b}$$

The same formulas apply for $J^s(p)$ if cos is replaced by sin. The two types of elementary integrals are given in Ref. 10, formulas 333:7b and 6b. After rearrangement, they take the forms

$$\tfrac{1}{2}J^c(p)=A\cos(kp)-kB\sin(kp)+k^2C\mathrm{Ci}(kp)$$

$$\tfrac{1}{2}J^s(p)=A\sin(kp)+kB\cos(kp)+k^2C\mathrm{si}(kp) \tag{A9}$$

The functions Ci and $\mathrm{si}\equiv\mathrm{Si}-\pi/2$ are the cosine and sine integrals (e.g., Ref. 11, formulas 5.2.1, 2 and 5). These may be calculated to very high accuracy by means of IBM Subroutine SICI, Ref. 12, p. 370.

Insertion of Eqs. (A9) into Eq. (A5) yields

$$w(x;k)=-A+ikB-k^2[\mathrm{Ci}(kp)-i\mathrm{si}(kp)]Ce^{ikp}$$

$$(x\leq -1) \tag{A10}$$

[If the argument kp is large, Ci and si may be expressed by the functions $f(z)$ and $g(z)$ (see formulas 5.2.8,9,34 and 35 of Ref. 5). Then

$$w(x;k)=-A+ikB-k^2[\mathrm{if}(kp)-g(kp)]C \tag{A10a}$$

No oscillatory term is left in this asymptotic form.]

The letters A, B, and C in Eqs. (A9) indicate series in k or double series in k and p. These series are

$$A=\sum_0^{\infty}k^{2n}A_n=\frac{1}{2p^2}\sum_0^{\infty}k^{2n}\sum_{\nu=0}^{\infty}(-)^\nu\frac{A_{n,\nu}}{p^{2\nu}} \tag{A11a}$$

$$B=\sum_0^{\infty}k^{2n}B_n=\frac{1}{2p}\sum_0^{\infty}k^{2n}\sum_{\nu=0}^{\infty}(-)^\nu\frac{B_{n,\nu}}{p^{2\nu}} \tag{A11b}$$

$$C=\sum_0^{\infty}k^{2n}C_n=\frac{1}{2}\sum_0^{\infty}k^{2n}\cdot\frac{\bar{n}}{(2n+2)!} \tag{A11c}$$

where

$$A_{n,\nu}=(2\nu+1)B_{n,\nu} \tag{A11d}$$

$$B_{n,\nu}=\frac{\overline{n+\nu}\cdot(2\nu)!}{(2n+2\nu+2)!} \tag{A11e}$$

Note that

$$2A_0=-1+(1+p^2)^{1/2}/p \tag{A12}$$

If one sets $k=0$ in Eq. (A10), all terms on the right disappear except $-A_0$, and the familiar steady flow result is recovered.

Since

$$A_{n,0}=B_{n,0}=C_n \tag{A13}$$

one can simplify by splitting off the terms $\nu=0$, setting

$$A=C/p^2-\bar{A} \tag{A13a}$$

$$B=C/p-\bar{B} \tag{A13b}$$

so that Eq. (A10a) becomes (again for $x\leq -1$)

$$w(x;k)=-\{1/p^2-ik/p+k^2[\mathrm{Ci}(kp)-i\mathrm{si}(kp)]e^{ikp}\}C$$

$$+\bar{A}-ik\bar{B} \tag{A14}$$

The factor C is quickly calculated:

$$C=\frac{1}{4}+\frac{k^2}{96}+\frac{k^4}{3840}+\frac{k^6}{258048}+\cdots \tag{A15}$$

Table A1 Coefficients in Eqs. (A16a) and (A16b)

	$p=1$	$p=2$	$p=3$	$p>3$
$\bar{A}_0$	0.042893	0.003483	0.000732	$1/16p^4 - 1/32p^6 + 5/256p^8$
$\bar{A}_1$	0.001227	0.000092	0.000019	$1/640p^4$
$\bar{A}_2$	0.000020	0.000001	0	0
$\bar{B}_0$	0.016420	0.002428	0.000747	$1/48p^3 - 1/160p^5$
$\bar{B}_1$	0.000448	0.000062	0.000019	$1/1920p^3$
$\bar{B}_2$	0.000007	0.000001	0	0

The series $\bar{A}$ and $\bar{B}$ we write as

$$\bar{A} = \sum_0^\infty k^{2n} \bar{A}_n(p) \tag{A16a}$$

$$\bar{B} = \sum_0^\infty k^{2n} \bar{B}_n(p) \tag{A16b}$$

Sample numerical values are given in Table A1; using these, one can quickly find $\bar{A}$ and $\bar{B}$ if $p=1$, 2, or ≥ 3. For intervening p values[§] only $\bar{A}_0$ and $\bar{B}_0$ may be required if k is small enough and/or if p is large enough. Of these, $\bar{A}_0$ can be calculated from its analytical form, compare Eq. (A12):

$$\bar{A}_0 = [1 + 1/2p^2 - (1 + 1/p^2)^{1/2}]/2 \tag{A17}$$

The series $\bar{B}_0$ converges slowly if p is close to 1, but still fast enough for modern computers. Alternately, one may calculate the part-integral $J(p,2)$ by numerical integration and determine the remaining integral using Table A1.

Case $x \geq +1$

If $x \geq +1$, then $x=p$, and from the symmetry properties of the circular functions, it follows that

$$J^c(-p) = 2J^c(0) - J^c(p) \tag{A18a}$$

$$J^s(-p) = J^s(p) \tag{A18b}$$

Therefore, Eq. (A5) takes the form

$$w(x;k)e^{ikx} = \tfrac{1}{2}J^c(x) - J^c(0) + (i/2)J^s(x) \qquad (x \geq +1) \tag{A19}$$

An alternate form of Eq. (A19) is sometimes useful:

$$w(x;k) = -\mathrm{Re}w(-x;k) + i\mathrm{Im}w(-x;k) - J^c(0)e^{-ixk} \tag{A19a}$$

Of the terms on the right of Eq. (A19), only the part-integral $J^c(0,1)$ has not already been discussed. For this integral, we have

$$-J^c(0,1) = -\int_0^1 \frac{\cos k\zeta \, d\zeta}{\zeta^2 (1+\zeta^2)^{1/2}} = \sum_0^\infty k^{2\nu} I_\nu \tag{A20}$$

The elementary integrals

$$I_\nu = \frac{(-)^{\nu+1}}{(2\nu)!} \int_0^1 \frac{\zeta^{2\nu-2} \mathrm{d}\zeta}{(1+\zeta^2)^{1/2}} \tag{A20a}$$

are standard integrals (e.g., Ref. 10, Sec. 234). Their numerical values converge to zero rapidly as ν increases (see Table A2).

[§] Noninteger values of p do arise, e.g., when $y \neq 0$.

Table A2 Elementary integrals I_ν in Eq. (A20a)

$I_0 = \sqrt{2}$	=	+1.414214
$I_1 = \tfrac{1}{2}\log(1+\sqrt{2})$	=	+0.440687
$I_2 = (2I_1 - \sqrt{2})/48$	=	−0.011101
$I_3 = (6I_1 - \sqrt{2})/5760$	=	+0.000214
$I_4 = (30I_1 - 13\sqrt{2})/1935360$	=	−0.000003

When x is large (and positive), the integral $J^c(0)$ provides by far the largest contribution to $w(x;k)$, Eq. (A19a), and this contribution is oscillatory. Herein lies a pronounced distinction between the ranges of large positive x and of large negative x, Eq. (A10a).

Case $|x| < 1$

Since the series Eqs. (A11b) and (A11c) are not all convergent when $p<1$, one has to calculate the part-integral $J(p,1)$ by some other means. Series presentation corresponding to Eq. (A20) can be used, but direct numerical quadrature is more convenient, except when k is quite small. Equations (A19) and (A19a) remain valid.

Case $y \neq 0$

When $y_n = 0$, the integral $J(-x)$, Eq. (A5), represents the sum of the two identical contributions, to the downwash $w(x,y_n;k)$ from the ranges $0 \leq \eta \leq 1$ and $-1 \leq \eta \leq 0$ of the system of vortices that is created by E_s. If $y_n \neq 0$, these two contributions differ. Using Eq. (A4a), one easily shows that, if y_n is positive,

$$w(x,y;k) = \frac{1}{2}\left[\frac{1}{y+1} w\left(\frac{x}{y+1};k(y+1)\right) - \frac{1}{y-1} w\left(\frac{x}{y-1};k(y-1)\right)\right] \tag{A21}$$

where y again stands for y_n. Furthermore, it is obvious that $w(x,-y;k) = w(x,y;k)$. Thus, Eq. (A21) is valid for negative y_n also if, on the right, y is read as $|y_n|$.

The fact that two w terms on the right of Eq. (A21) have to be calculated to obtain one w term on the left is offset by the fact that (almost all) the w terms on the right serve with two values y_n. Thus, the apparent doubling of the required numerical effort does not actually occur.

Rectangular Elements

For the calculations reported in the main part of this paper, rectangular wings of aspects ratio A were divided into $N \times N$ rectangular elements of aspect ratio A. This pattern then replaces Fig. A1, but we may leave the x coordinate invariant, still referred to the length l, where $2l$ is still the chordlength of the element, and Eq. (A1) remains valid. Also in order to leave the characteristic integers y_n invariant, we have to refer the spanwise coordinate to the length lA. Then Eq. (A21) becomes

$$w_A(x,y;k) = \frac{1}{2A}\left[\frac{1}{y+1} w\left(\frac{x}{(y+1)A};kA(y+1)\right) - \frac{1}{y-1} w\left(\frac{x}{|y-1|A};kA|y-1|\right)\right] \tag{A22}$$

Equation (A22) is correct also for $y=0$.

Review

The problem is to calculate aerodynamic influence coefficients $w(x,y;k)$ by means of Eqs. (A4) and (A4a). In our method, in contrast to earlier, approximate methods, the spanwise integration, Eq. (A4), is performed first and is performed analytically; the subsequent streamwise integration to infinity, Eq. (A4a), is also performed analytically and leads

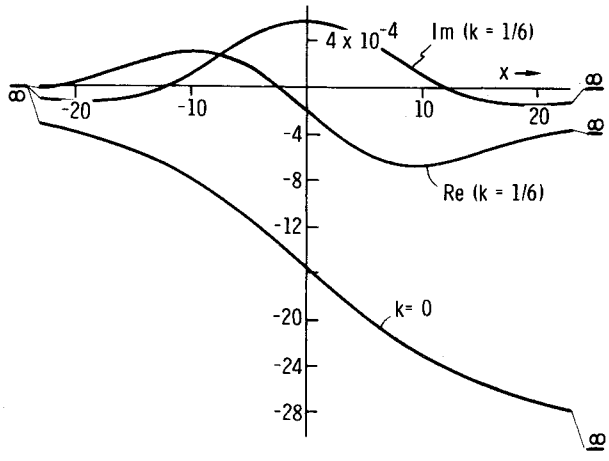

Fig. A2 Sample steady and unsteady influence functions: $w(x,18;k)\exp(ixk)$.

to a pair of real-valued functions of a single parameter (the functions $\mathrm{Ci}(kp)$ and $\mathrm{si}(kp)$ in Eqs. (A9)) which can readily be calculated to practically arbitrary accuracy.

In addition, the series A, B, and C and Eq. (A20a) have to be evaluated. This does not pose any problem if $k \leq 1$ in $w(x;k)$ since, in this case, Tables A1 and A2 suffice for sixth decimal accuracy (apart from rounding-off errors)—a considerable accuracy in view of the fact that, because of our definition of w, Eq. (A3), the largest influence coefficient in the matrix is 0(1).

However, in calculating $w(x,y;k)$, the effective values of the parameters of the functions $w(x_{\mathrm{eff}}; k_{\mathrm{eff}})$ on the right of Eq. (A22) differ considerably from the values x and k on the left. From Eq. (A1), we have

$$k_{\mathrm{eff,max}} = 2Ak_{c/2}(1 - 1/2N) \tag{A23}$$

for the largest value of k_{eff} that occurs in the matrix. While with flutter coefficients the required values $k_{c/2}$ are often fairly small and the condition $k_{\mathrm{eff}} \leq 1$ may well be fulfilled, we required gust load results for higher $k_{c/2}$. Fortunately, all four series just listed converge with accelerating rapidity. Using only three more terms in each, we achieved sixth decimal accuracy up to $k_{\mathrm{eff}} = \sqrt{10}$, and achieved the same accuracy for the final coefficients, $w(x,y;k)$, with even higher k_{eff} because of the small factors with the w on the right of Eq. (A22).

In many cases $|x_{\mathrm{eff}}|$ is smaller than 1 and $J(p,1)$ has to be calculated by numerical quadrature or by some other means (see above). In performing the quadrature, one has to be careful to retain sufficient accuracy in spite of the ζ^2 in the denominator, Eq. (A5). On the other hand, the fact that $J^c(p,1)$ increases like $(1/p)$ when p becomes small is not of concern, since this increase is offset by the small factors with the w on the right of Eq. (A22).

This concludes our review of the aerodynamic analysis methods by which our influence coefficients have been determined. Sample influence functions, for $A=1$, $y=18$, and $k=0$ and $k=1/6$, are shown in Fig. (A2) to illustrate their nature. One sees that, away from the x axis, the unsteady influence field is much weaker than the steady field. Thus, even with a k value as small as $k=1/6$, the former can hardly be considered a minor perturbation of the latter.

Acknowledgments

The research reported here was sponsored by the Air Force Office of Scientific Research (AFSC), United States Air Force, under Contract F44620-73-C-0041. Program Manager and Technical Monitor was M. Rogers. C. Hutton designed and prepared the computer program and was responsible for performing the computer calculations.

References

[1] Jordan, P.F., "Integration of the 3-D Harmonic Kernel," AFOSR-TR-0948, Aug. 1976.

[2] Thwaites, B., *Incompressible Aerodynamics,* Clarendon Press, Oxford, 1960.

[3] Hedman, S.G., "Vortex Lattice Method for Calculation of Quasi Steady State Loadings on Thin Elastic Wings," Aeronautical Research Institute of Sweden, Rept. 105, Oct. 1965.

[4] Woodward, F.A., "Analysis and Design of Wing-Body Combinations at Subsonic and Supersonic Speeds," *Journal of Aircraft,* Vol. 5, Nov.-Dec. 1968, p. 528.

[5] Graham, J.M.R., "A Lifting Surface Theory for the Rectangular Wing in Non-Stationary Flow," *Aeronautical Quarterly,* Vol. 12, Feb. 1971, p. 83.

[6] Jones, R.T., "The Unsteady Lift of a Wing of Finite Aspect Ratio," NACA TR 681, 1940.

[7] Murrow, H.N., Pratt, K.G., and Drischler, J.A., "An Application of a Numerical Technique to Lifting-Surface Theory for Calculation of Unsteady Aerodynamic Forces due to Continuous Sinusoidal Gusts on Several Wing Planforms at Subsonic Speeds," NASA TN D-1501, 1963.

[8] Giesing, J.P., Kalman, T.P., and Rodden, W.P., "Subsonic Unsteady Aerodynamics for General Configurations," AFFDL-TR-71-5, Pt. I, Vol. I, Nov. 1971.

[9] Jordan, P.F., "Numerical Evaluation of the 3-D Harmonic Kernel," AFOSR-TR-76-0004, Aug. 1975; *Z. Flugwissenschaften,* Vol. 24, July-Aug. 1976, p. 205.

[10] Gröbner, W. and Hofreiter, N., *Integraltafel,* Pt. I, Springer, Wien, New York, 1965.

[11] Abramowitz, M. and Stegun, I.A. (eds.), *Handbook of Mathematical Functions,* 3rd prtg., National Bureau of Standards, 1965.

[12] IBM Systems/360 Scientific Subroutine Package, Aug. 1970.